AppliedChem

MDPI

Article

The Facile Microwave-Assisted Coprecipitation Route to Obtain Polyoxoniobate ($Na_7(H_3O)Nb_6O_{19}{\cdot}14H_2O$) Nanorods Modified with Copper for CO_2 Photoreduction

Joelma R. C. Souza [1], Juliana A. Torres [2], Lucas S. Ribeiro [3], Jose B. G. Filho [1], Fabiana L. Santos [1], Nicholas Malgioglio [4], Luiz Fernando Gorup [3,5,6], Alexandre H. Pinto [4,*] and André E. Nogueira [1,*]

1 Department of Chemistry, Institute of Exact and Biological Sciences (ICEB), Federal University of Ouro Preto—UFOP, Ouro Preto 35400-000, Brazil
2 Embrapa Instrumentation, São Carlos 13560-970, Brazil
3 Interdisciplinary Laboratory of Electrochemistry and Ceramics (LIEC), Department of Chemistry, UFSCar—Federal University of São Carlos, São Carlos 13565-905, Brazil
4 Department of Chemistry & Biochemistry, Manhattan College, 4513 Manhattan College Parkway, Riverdale, NY 10471, USA
5 Institute of Chemistry, Federal University of Alfenas, Alfenas 37130-001, Brazil
6 School of Chemistry and Food Science, Federal University of Rio Grande, Rio Grande 96203-900, Brazil
* Correspondence: alex.pinto@manhattan.edu (A.H.P.); andre.esteves@ufop.edu.br (A.E.N.); Tel.: +55-71-8862-7211 (A.H.P.); +55-31-3559-1707 (A.E.N.)

Abstract: The CO_2 reduction by solar means has been discussed as an alternative to emission abatement, a fundamental topic for sustainable, carbon-free production in the future. However, the choice of efficient systems, starting with the catalysts, is still a critical issue, especially due to the poor activity of available options. Polyoxometalates have been extensively studied as promising photocatalysts due to their semiconducting properties. Nevertheless, the synthetic conditions of polyoxoniobate are stringent due to the low reaction activity of Nb species, the lack of soluble precursors, and the narrow pH range. Unlike the literature, in the present study, we report a simple polyoxoniobate synthesis method. This synthesis method has some remarkable features, such as low processing time and temperature and good activity and selectivity in the CO_2 photoreduction process. The results revealed an outstanding efficiency for the CO_2 reduction reaction with a high selectivity of CO_2 to CO conversion (92.5%). Furthermore, C2 compounds (e.g., acetate) were produced in the liquid phase of the reaction system. Our findings are significant for indicating the potential of polyoxoniobate for CO_2 photoreduction, which opens a way to control competitive reactions with synthesis, leading to higher selectivity.

Keywords: polyoxometalates; microwave-assisted hydrothermal synthesis; photocatalysis; greenhouse gas

Citation: Souza, J.R.C.; Torres, J.A.; Ribeiro, L.S.; Filho, J.B.G.; Santos, F.L.; Malgioglio, N.; Gorup, L.F.; Pinto, A.H.; Nogueira, A.E. The Facile Microwave-Assisted Coprecipitation Route to Obtain Polyoxoniobate ($Na_7(H_3O)Nb_6O_{19}{\cdot}14H_2O$) Nanorods Modified with Copper for CO_2 Photoreduction. *AppliedChem* **2023**, *3*, 320–333. https://doi.org/10.3390/appliedchem3020020

Academic Editor: Jason Love

Received: 16 February 2023
Revised: 7 June 2023
Accepted: 7 June 2023
Published: 12 June 2023

1. Introduction

The conversion of CO_2 into compounds with higher added value, mainly in compounds with high energy value, is an approach with enormous potential, promoting the philosophy of circular economy, which describes one of the largest sustainability models of today [1,2]. Thus, developing processes that add value to greenhouse gases, such as CO_2, is one of the most promising strategies for reducing and controlling these gases in the atmosphere.

Currently, the conversion of CO_2 into fuels such as methane, ethanol, and isopropanol can be achieved through different processes, such as photochemical [3], thermochemical [4], electrochemical, and photo-electrochemical [5] processes, in which each process uses one or more energy sources to enable the reduction of CO_2.

Although high-temperature technologies are favored from a thermodynamic and kinetic point of view, their implementation involves problems that are difficult to solve in the management of the heat involved in the reaction. As such, several efforts are currently devoted to the development of low-temperature technologies, such as photocatalytic and photoelectrocatalytic CO_2 reduction processes, which hold enormous potential to convert CO_2 into different compounds using energy from renewable sources such as solar radiation [5,6]. However, the efficiency of photocatalytic processes is currently still quite limited, which makes its application on an industrial scale impossible. In this scenario, advances in the processes of developing new photocatalysts to promote these reactions are essential. In the specific case of CO_2 photoreduction, the choice of the most suitable materials plays a central role since they must have a good affinity with the CO_2 molecule, good stability, and an adequate conduction band potential to allow the reduction of this molecule.

Thus, the polyoxometalates (POMs) of some transition metal elements, such as tungsten, vanadium, molybdenum, and niobium, have arisen considerable interest due to their unique structural properties and their peculiar chemical reactivity. These features open up new paths for the development of multifunctional materials, for catalysis applications, in photo and electrochromic devices, and for medicine and materials science [7–10]. The fundamental properties of the polyoxometalates, such as elemental composition, solubility, redox potential, load density, size, and shape, can be systematically altered to a considerable degree [11].

Among the POMs, polyoxoniobates are very poorly explored compared to polyoxotungstates, vanadates, and molybdates, which are more easily formed over a wide pH range simply with acidification. Additionally, their polyoxoanions can be easily fused at ambient pressures and temperatures [12,13]. The polyoxoniobates, on the other hand, have strict synthetic conditions because of the low-reaction activity of Nb species, the lack of soluble precursors, and the narrow pH range.

Lindqvist first reported the structure of the Lindqvist-type hexaniobate anions $[Nb_6O_{19}]^{8-}$ in 1953. Many of the catalytic properties of this material come from its redox potential since they have a high capacity to release and transport electrons and can be considered as weak Lewis bases due to the presence of superficial oxo groups that can bind easily with Lewis acids [14–16].

Regarding these mentioned features, polyoxoniobate has been widely used as an efficient catalyst and support for semiconductor nanostructures and organic/inorganic molecules, presenting high catalytic and photocatalytic activity, both in the environmental remediation process and CO_2 photoreduction process and in catalytic oxidation reactions, to obtain compounds with higher added value [9,17–19]. Shen et al. reported the synthesis of two three-dimensional (3D) photocatalysts based on polyoxoniobate and tantalum and applied them in the photodegradation process of methylene blue dye. The photocatalytic reaction showed that the dye can be effectively degraded using the 3D photocatalyst and that the degradation efficiency depends on the pH, reaction time, concentration of the dye solution, and type of anions present in the photocatalyst structure [20].

In another work, Heng et al. developed a heterostructured photocatalyst of polyoxidoniobate and graphene through the solvothermal method for the degradation of the antibiotic tetracycline. The results showed that the formed heterostructure presented high stability, recyclability, and excellent photocatalytic activity, reaching 74.69% degradation in just 9 min. In addition, it was verified that the formation of the heterojunction helped in the separation of the photogenerated electron-hole pairs and in the charge transfer, leading to greater efficiency of the photocatalytic process [21].

Photocatalytic reactions can not only be used in the degradation process of countless and varied organic pollutants but can also be applied in energy generation, such as in the production of H_2 and the reduction of CO_2 into CH_4, ethanol, and methanol, among other products of greater energetic value. During the process, while the photogenerated holes (h^+) will drive oxidation reactions, the electrons (e^-), in turn, will drive reduction reactions.

Huang et al. synthesized and characterized three structures of polyoxidoniobates: (i) $KNa_2[Nb_{24}O_{72}H_{21}]\cdot 38H_2O$, (ii) $K_2Na_2[Nb_{32}O_{96}H_{28}]\cdot 80H_2O$, and (iii) $K_{12}[Nb_{24}O_{72}H_{21}]_4\cdot 107H_2O$, and verified the photocatalytic activities of H_2 evolution under ultraviolet radiation (UV). Through the UV-vis diffuse reflectance spectra, the band-gap energy was determined, with the values found for structures i, ii, and iii being 3.35, 3.17, and 3.34 eV, respectively, highlighting the semiconductor nature of the materials. The evaluation of the photocatalytic activities in the H_2 generation process under UV radiation was performed using the $Co^{III}(dmgH)_2pyCl$ complex as a cocatalyst and triethylamine (TEA) as a sacrificial electron donor. The H_2 evolution rate in three cycles was 5161.4, 5233.5, and 5186.7 μmol h^{-1} g^{-1} for material i, 5312.5, 5032.5, and 4824.3 μmol h^{-1} g^{-1} for material ii, and 4804.1, 4802.3, and 4537.7 μmol h^{-1} g^{-1} for material iii. After 12 h of reaction, materials i, ii, and iii produced 6232.7, 6069.6, and 5657.6 μmol of hydrogen, respectively. In addition to good photocatalytic activity, when these materials were kept at room temperature for a long time after the photocatalytic process, no significant changes in their band structure were observed, suggesting that these photocatalysts are stable [22].

Motivated by the photocatalytic efficiency and the laborious synthesis reported in the literature for such materials, the purpose of this study was to develop a high-performance copper-modified polyoxoniobate catalyst with suitable properties for applications in the CO_2 photoreduction process using a quite convenient microwave-assisted hydrothermal synthesis route. The catalyst preparation method used in this study proved to be extremely efficient for producing polyoxoniobate nanorods in a short period of time and at low temperatures, and it turned their activities toward CO_2-selective reduction.

2. Materials and Methods

2.1. Synthesis of the Polyoxoniobate Pure and Modified with Copper

The synthesis of $Na_7(H_3O)Nb_6O_{19}\cdot 14H_2O$ modified with copper was performed using the microwave-assisted coprecipitation method. The initial stage of the synthesis consisted of the preparation of the niobium ammoniacal oxalate solution, in which 14 g (0.043 mol) of niobium ammonium oxalate ($(NH_4)[NbO(C_2O_4)2.4(H_2O)]$) and 4.74 g (0.02 mol) of $Cu(NO_3)2.3H_2O$ were added to 200 mL of H_2O. This solution had a concentration of 0.215 mol/L and 0.100 mol/L of niobium and copper, respectively, which resulted in a 2.15 mole ratio between Nb/Cu.

Then, this solution was heated to 80 °C under constant stirring until complete dissolution of the precursors, and 50 mL of aqueous NaOH 1 M solution was added. The pH of the solution was adjusted by adding NaOH 5 M up to pH 14. The formed precipitate was transferred to a 100 mL polytetrafluoroethylene capsule in a microwave reactor. Microwave-assisted hydrothermal-treatment temperatures ranged from 80 to 150 °C for 20 and 30 min. After treatment, the solution was cooled to room temperature, centrifuged, washed with H_2O, and dried in an oven at 60 °C for 12 h. The samples were conveniently named according to the time and temperature of the microwave-assisted hydrothermal treatment. The materials treated for 20 and 30 min at 150 °C were called Cu-PON-150 °C/20 min and Cu-PON-150 °C/30 min, respectively, and the materials treated for 30 min at 80 and 100 °C were called Cu-PON-80 °C/30 min and Cu-PON-100 °C/30 min, respectively. The polyoxoniobate without Cu^{+2} modification was prepared with the same experimental procedure, only excluding the $Cu(NO_3)2.3H_2O$ addition step. In this case, the material was heat-treated at 150 °C for 30 min and called PON-150 °C/30 min.

2.2. Characterization

Powder X-ray diffraction (XRD) patterns were obtained in the 5–60° range using CuK radiation (=0.15406 nm) on a Shimadzu XRD 6000 (Kyoto, Japan) at a rate of 0.5° min^{-1}. The amount of Cu present in the samples was determined with flame atomic absorption spectroscopy (FAAS) using a PerkinElmer (Waltham, MA, USA) model PinAAcle 900T. The flame was composed of synthetic air (10 mL) and acetylene (2.5 mL), and the absorbance was recorded using a Cu hollow cathode lamp with a characteristic wavelength

of 324.75 nm. The morphology of the materials was investigated using field emission scanning electron microscopy (JEOL JSM 6510, (Tokyo, Japan)). The band gaps were determined using the Tauc method [20] from diffuse reflectance (DRS) spectra (Shimadzu UV-2600) in the ultraviolet-visible region. Infrared (IR) spectra were obtained with a Fourier transform spectrophotometer (Bruker VERTEX 70, (Billerica, MA, USA)) with a range of 4000–400 cm^{-1}. The X-ray phototelectron spectroscopy (XPS) was carried out using a Thermo Fisher Scientific (Waltham, MA, USA) spectrometer, using Al-K alpha X-rays in vacuum (>108 mbar) and charge compensation during measurements. A resolution of 1 eV with 5 scans was used to gather the survey spectra, whereas the high-resolution spectra were recorded with 0.1 eV resolution and 50 scans. The binding energy was referenced to the C 1 s peak at 284.8 eV. Data analysis was performed using the Casa XPS software version 2.3.15.

2.3. Photoreduction Tests

The CO_2 photoreduction reactions were carried out in 150 mL quartz tubes with a septum for collecting gas and a capillary for CO_2 purge. To ensure the homogeneity of the reaction mixture, the tubes were inserted in a box linked to a thermostatic bath with an internal temperature of 15 °C and a magnetic stirrer. In addition to the water flow, airflow was used to cool down the box's interior, and the reactions were exposed to UV-C light from six UV-C lamps (Osram, 15 W, 254 nm, (Munich, Germany)). Then, a high-purity CO_2 flow was kept for 10 min to saturate the system with 100 mg of samples in 100 mL of distilled water. After 5 h of reaction, 400 µL aliquots of the headspace were extracted, and the products were analyzed on a gas chromatographer (Thermo Trace 1310) equipped with a capillary column (Carboxen 1010 PLOT (Sigma Aldrich, Burlington, MA, USA)). The detection was performed with flame ionization (FID) and thermal conductivity (TCD) detectors (set at 150 and 200 °C, respectively) using argon as the carrier gas. The products obtained in the liquid phase were identified and quantified using 1H nuclear magnetic resonance (NMR) (600 MHz, Ascend™ 600 Bruker) at 25 °C. For that, 540 µL of the sample was mixed with 20 µL of D_2O solution containing 5 mM dimethyl sulfoxide (DMSO) as an internal standard and 0.21 mM TSPd4 as a reference. The water peak was suppressed using a WET procedure, and the NMR data were processed using the MestreNova software. Before analyzing the activities of the material, blank tests were conducted to make sure that the data gathering and interpretation were not biased. Three experiments were conducted to determine whether some carbonaceous species from the materials' synthesis precursors affected the CO_2 photoreduction process: (1) without light (catalyst, water, and CO_2); (2) without CO_2 (catalyst, water, and light); and (3) without catalyst (water, CO_2, and light). Small amounts of CO and CH_4 were detected in tests ii and iii, but these results were appropriately disregarded. Consequently, the stability of the photocatalysts can be confirmed.

3. Results and Discussion

3.1. Cu-PONs Structural Characterizations

The high content of both Na^+ and OH^- ions in the synthesis solution led to the formation of $Na_7(H_3O)Nb_6O_{19}{\cdot}14H_2O$ while inhibiting the formation of more stable phases, such as $NaNbO_3$ [19,23].

$$3Nb_2O_5 + 8OH^- \rightarrow Nb_6O_{19}^{8-} + 4H_2O \quad (1)$$

$$Nb_6O_{19}^{8-} + 7Na^+ + 16H_2O \rightarrow Na_7(H_3O)Nb_6O_{19}{\cdot}(H_2O)_{14} + OH^- \quad (2)$$

Equation (1) illustrates that the synthesis process benefited from an excess of OH^- ions and thermal treatment with microwave radiation. This resulted in the increased solubility of niobium oxide species and facilitated the adsorption of hydroxyl anions on the surface

due to the affinity between Nb=O and O-H groups. Ultimately, this led to the production of the Lindqvist structure $[Nb_6O_{19}]^{8-}$ [24].

The diffractograms of the catalysts obtained at different times and temperatures (Figure 1) of microwave-assisted hydrothermal treatments show that all catalysts had the same crystalline structure related to the orthorhombic phase of hydrated sodium niobate with stoichiometry $Na_7(H_3O)Nb_6O_{19}{\cdot}14H_2O$ (ICSD N°: 038027). No diffraction peaks related to other niobium compounds were observed, indicating the lack of additional phases such as $NaNbO_3$ and $CuNb_2O_6$ [25]. Furthermore, no peaks related to copper phases, such as CuO and $Cu(OH)_2$, were identified.

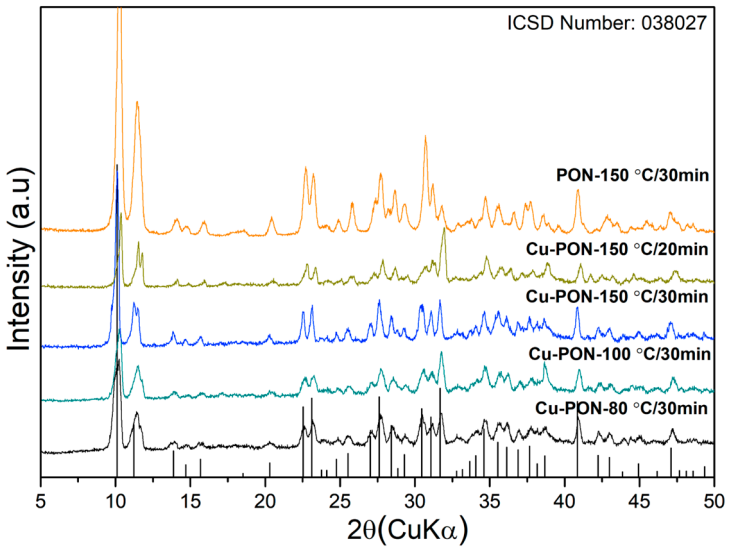

Figure 1. XRD of catalysts treated at different times and temperatures.

The FTIR spectra of the materials (Figure 2) show six vibrational modes from 400 to 900 cm^{-1}, which are related to the hexaniobate anion structure $[Nb_6O_{19}]^{8-}$ [22,26]. In the spectra, the bands at 867 and 840 cm^{-1} are assigned to the terminal Nb-O vibration, and the bands between 800 and 400 cm^{-1} are assigned to the bridged Nb-O-Nb vibration. The spectral features around 840, 770, 510 and 430 cm^{-1} indicate that the catalysts have a Lindqvist-type structure $[Nb_6O_{19}]^{8-}$ [22,26].

Figure 3 shows the UV−Vis spectra of catalysts synthesized at different synthesis times and temperatures. The materials PON-150 °C/30 min, Cu-PON-80 °C/30 min, Cu-PON-100 °C/30 min, and Cu-PON-150 °C/30 min showed a band gap value between 3.20 and 3.40 eV; however, the Cu-PON-150 °C/20 material showed a shift to a lower energy value of 2.60 eV (Table 1). It is important to emphasize that this broad absorption observed in the UV and visible regions confirms the possible application of the catalyst in photocatalytic processes under visible radiation.

Table 1. Band gap energy values and the mole percentage of copper in the synthesized materials treated at different times and temperatures.

Materials	Band Gap (eV)	%Cu *
PON-150 °C/30 min	3.36	-
Cu-PON-150 °C/20 min	2.60	6.99
Cu-PON-80 °C/30 min	3.40	10.05
Cu-PON-100 °C/30 min	3.30	10.65
Cu-PON-150 °C/30 min	3.20	11.76

* %Cu: mass percentage of Cu present in the material obtained with AAS.

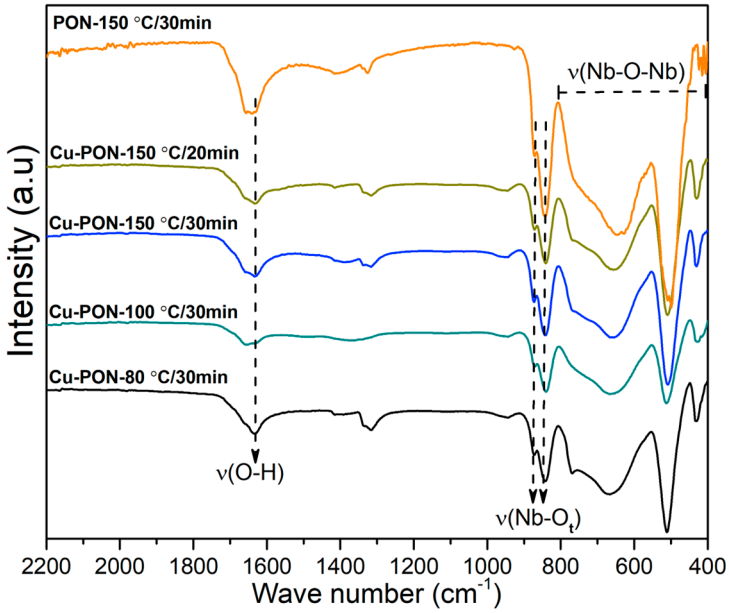

Figure 2. Infrared spectra of materials synthesized at different times and temperatures.

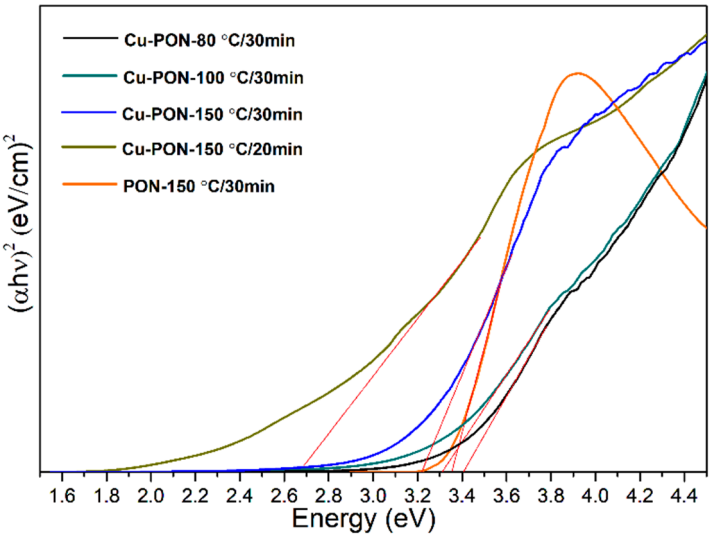

Figure 3. Band gap energy of the PON-150 °C/30 min and the catalysts modified with Cu.

The copper content present in the synthesized materials was determined using the atomic absorption spectrometry technique (Table 1). Among the materials, the one synthesized at 150 °C for 20 min showed a lower Cu content in its structure of approximately 7.0%.

To verify the morphology of the materials synthesized at different times and temperatures, scanning electron microscopy (SEM) was used (Figure 4). All materials showed rod-shaped particles with nanoparticles on their surfaces, with no significant difference in morphology with the variation of time and temperature of crystallization in the microwave-assisted hydrothermal process. Table 2 presents the length and width for all the materials prepared, obtained from particle size distribution using SEM images. The materials showed an average particle length roughly between 5 and 9 μm, whereas the width ranges between 1.1 and 1.8 μm. There is no clear correlation between the average particle size and temperature or time of the heating treatment. Additional SEM images of these materials and the histograms of the particle size distribution can be found in Figures S4–S9 in the supplementary materials File.

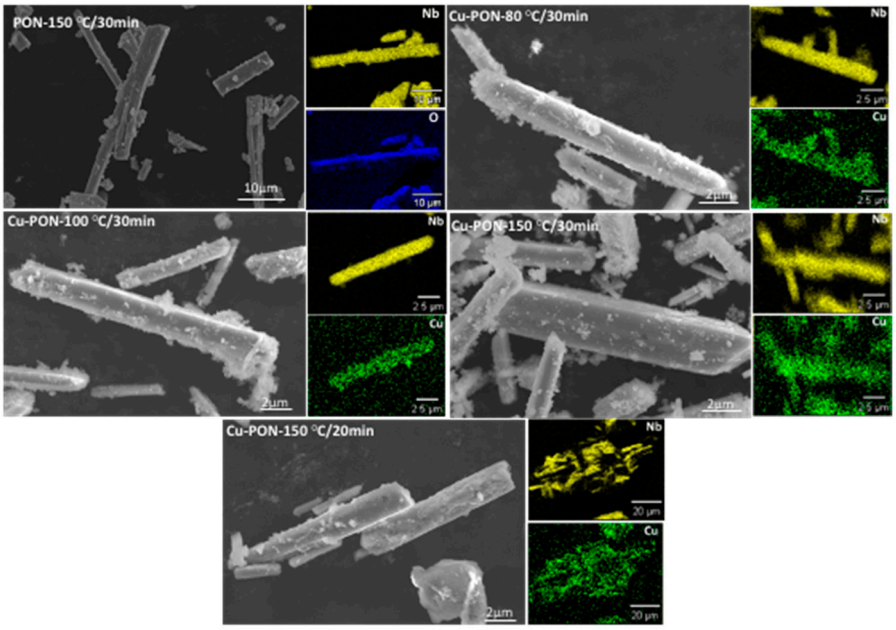

Figure 4. Scanning electron microscopy (SEM) images and EDS mapping images of materials synthesized at different temperatures (80 °C, 100 °C, and 150 °C) and times (20 and 30 min).

Table 2. Particle size with length, width, and aspect ratio.

Materials	Length Particle Size (µm) *	Width Particle Size (µm) *	Aspect Ratio *
PON 150 °C/30 min	7.33 ± 3.49	1.74 ± 0.55	4.20
Cu-PON 150 °C/20 min	5.43 ± 1.73	1.26 ± 0.36	4.31
Cu-PON 80 °C/30 min	9.09 ± 4.30	1.38 ± 0.43	6.58
Cu-PON 100 °C/30 min	6.06 ± 3.00	1.22 ± 0.46	4.97
Cu-PON 150 °C/30 min	5.04 ± 2.43	1.08 ± 0.36	4.67

* Particle size: the average particle size was determined from the SEM images using ImageJ software version 1.53k.

To obtain the distribution of elements in the material, the EDS mapping technique was applied, and the results showed a homogeneous distribution of Cu in the material structure. Based on the EDS mapping of the catalysts and the copper content values in the structure, it can be concluded that copper is functioning as a dopant rather than solely as a counter-ion. Aiming to obtain further information about whether the Cu^{+2} would behave as a dopant or counter-ion, we performed an X-ray photoelectron spectroscopy (XPS) analysis on the sample Cu-PON 150 °C/30 min, as shown in Figure S13 of the supplementary materials File. The XPS analysis of the Cu2p band indicated that the copper is found as Cu^{+2} in this sample. This information indicates that there was no reduction of Cu^{+2} to metallic copper during the polyoxoniobate preparation. However, it does not provide definite information about whether the Cu^{+2} would behave as a dopant or counter-ion.

Although none of the characterization techniques provide definite proof that the Cu^{+2} works as a dopant instead of a counter-ion, we believe there is strong evidence of the dopant behavior. For instance, if copper were only present as a counter-ion, the high concentration of hydroxide in the medium would cause the Cu^{2+} ion to react and form copper oxide (CuO) due to its susceptibility to oxidation [27]. However, the diffractograms of all catalysts, which contained more than 5 wt% of copper, only showed peaks related to the polyoxoniobate phase and not the CuO phase. These results suggest that copper is evenly distributed throughout the crystalline structure, similar to Nb, which was verified with EDS analysis.

3.2. CO_2 Photoreduction

POMs are a vast class of inexpensive, stable transition-metal oxygen photocatalysts that exhibit semiconductor-like photochemical behaviors due to intrinsic electronic charac-

teristics. The potential of copper-modified polyoxoniobate was evaluated in the process of CO_2 photoreduction under UV radiation in the presence of water (Figure 5).

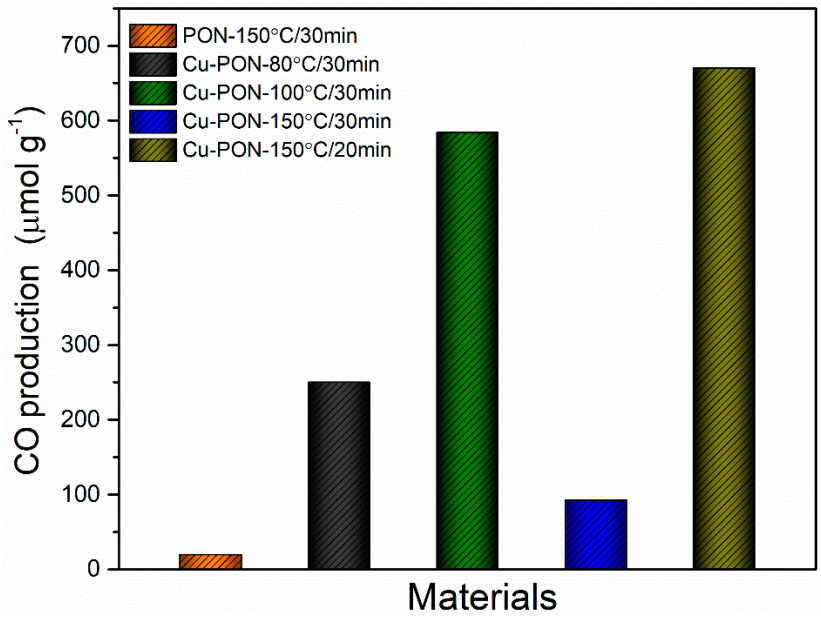

Figure 5. CO evolution in the CO_2 photoreduction under UV radiation after 5 h of reaction.

In the gaseous phase of the photoreactor, we observed the formation of CO and CH_4, 18.6 μmol.g^{-1} and 0.8 μmol.g^{-1}, respectively, using the PON-150 °C/30 min. However, with copper-modified materials, only CO formation was detected. The catalysts PON-150 °C/20 min and PON-100 °C/30 min proved to be more efficient for converting CO_2 to CO compared to the other materials synthesized, producing approximately 670 μmol.g^{-1} and 584 μmol.g^{-1} of CO after 5 h of reaction under UV radiation, respectively, while the material PON-150 °C/30 min was the least efficient for the production of CO through the photoreduction process, producing only 93 μmol.g^{-1}.

Due to the high activity of the materials modified with copper, an analysis of the products formed in the aqueous part of the reactor was carried out with NMR. Figure 6 shows the products formed in the photoreduction process in an aqueous medium after 5 h of reaction under UV radiation. Only acetate and formate were detected (see the ^{1}H NMR spectra shown in Figures S2–S4). Acetate/formate yields are 27.3/0.0 μmol.g^{-1}, 22.2/7.7 μmol.g^{-1}, 27.5/8.4 μmol.g^{-1}, and 18.6/17.1 μmol.g^{-1} for PON-80 °C/30 min, PON-100 °C/30 min, PON-150 °C/30 min, and PON-150 °C/20 min, respectively.

Equation (3) was used to determine the number of electrons engaged in the CO_2 photoreduction. According to the number of the electron transmitted in the processes (Equations (4)–(6)) per CO_2 mole, the coefficients multiplying the production rates were estimated [28]:

$$n_{e^-} = (2 \times n_{CO}) + (2 \times n_{HCOOH}) + (4 \times n_{CH_3COOH}) \quad (3)$$

$$CO_{2(g)} + 2\,e^- + 2\,H^+{}_{(aq)} \rightarrow CO_{(g)} + H_2O_{(l)}\ 2e^-/mol_{CO_2} \quad (4)$$

$$CO_{2(g)} + 2e^- + 2H^+{}_{(aq)} \rightarrow HCOO^-_{(aq)} + 5\,H_2O_{(l)}\ 2e^-/mol_{CO_2} \quad (5)$$

$$2CO_{2(g)} + 8\,e^- + 8\,H^+{}_{(aq)} \rightarrow CH_3COO^-_{(aq)} + 2H_2O_{(l)} 4e^-/mol_{CO_2} \quad (6)$$

where n is the amount of CO, $HCOO^-$, and CH_3COO^- in micromoles per gram of material for every mole of CO_2, respectively.

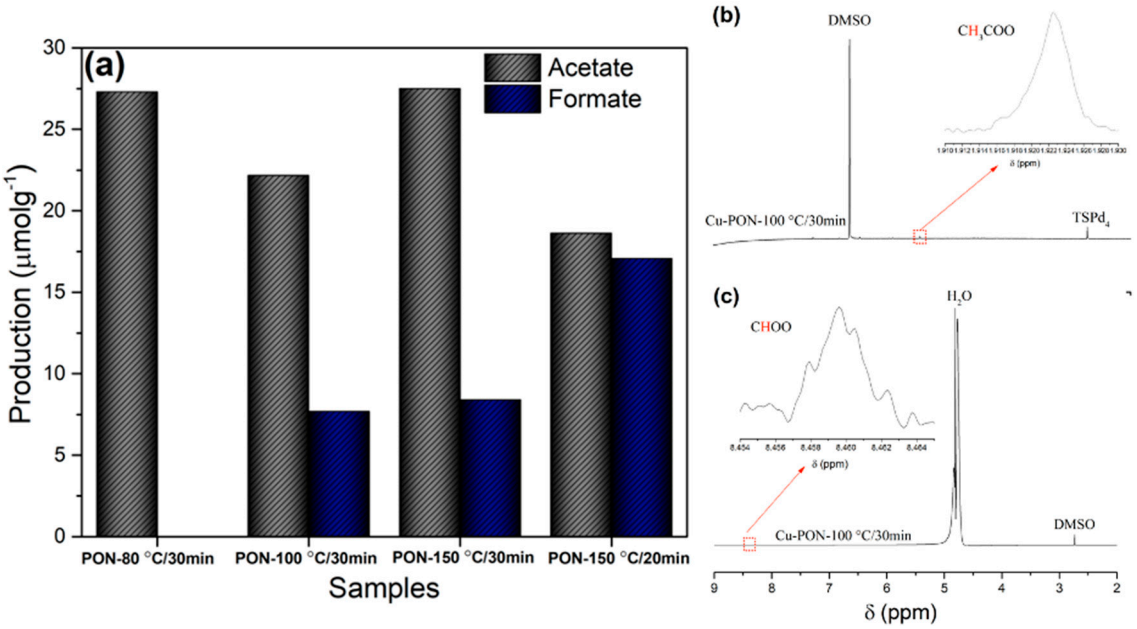

Figure 6. Products formed in the liquid medium during the CO_2 photoreduction process after 5 h of reaction under UV radiation (**a**), and the NMR spectrum of the products with Cu-PON-100 °C/30 min: (**b**) acetate, and (**c**) formate. Insets in figures (**b**,**c**) show an enlarged view of the spectrum.

Figure 7b shows that PON-150 °C/20 min exhibited the highest activity, with a total number of electrons involved per CO_2 reduction of 1449.52 e^-, followed by PON-100 °C/30 min with 1272.48 e^-. Despite the catalysts showing significant differences in the photocatalytic production of organic acids, all of them showed high selectivity for carbon monoxide, reaching a maximum of 92.5% for the PON 150 °C/20 min. This selectivity of 92.5% for CO is relatively high when compared with the CO selectivity obtained by other papers in the literature using POMs as part of the photocatalysts for the CO_2 photoreduction reaction, as can be seen in Table 3:

Table 3. List of POM-based photocatalysts used for CO_2 photoreduction with CO selectivity.

Photocatalyst	POM Composition	Medium	Radiation	CO Selectivity	Reference
Cu-modified polyoxoniobate	$Na_7(H_3O)Nb_6O_{19}{\cdot}14H_2O$	High-purity CO_2 purged into deionized water	UV-radiation (254 nm)	92.5%	This work
Mo-based MOF prepared via POM induction	$Zn_2Co_2(MoO_4)(HCO_2)_3(C_4H_5N_2)_3{\bullet}DMF$ (Zn/Co/Mo MOF)	Gaseous pure CO_2 medium with MeCN solvent, $[Ru(bpy)_3]Cl_2$ photosensitizer and TEOA sacrificial agent	Visible light	91.4%	[29]
Mo-based MOF prepared via POM induction	$Zn_4(MoO_4)(HCO_2)_3(C_4H_5N_2)_3{\bullet}DMF$ (Zn/Mo MOF)	gaseous pure CO_2 medium with MeCN solvent, $[Ru(bpy)_3]Cl_2$ photosensitizer and TEOA sacrificial agent	Visible light	72.8%	[29]
The POM with composition $K_4Na_{28}[\{Co_4(O\text{-}H)_3(VO_4)\}_4(SiW_9O_{34})_4]$ $66H_2O$	$K_4Na_{28}[\{Co_4(O\text{-}H)_3(VO_4)\}_4(SiW_9O_{34})_4]$ $66H_2O$	The substrate was CO_2 saturated in CH_3CN/H_2O as solvent. Using TEOA as sacrificial agent and $[Ru(phen)_3]$ as photosensitizer	450 nm LED ligh	99.6%	[30]
POM-based host–guest organo–metallophosphate (OMPO) frameworks	$[Zn_4(PO_4)(C_7H_8N_4)_6]$ $[BW_{12}O_{40}]{\bullet}2H_2O$	High purity CO_2 was the substrate. The CH_3CN was the solvent. TEOA was the sacrificial agent, and $[Ru(bpy)_3]Cl_2$ was the photosensitizer	Visible light	64.6%	[31]
POM-based host–guest organo–metallophosphate (OMPO) frameworks	$[Co_4(PO_4)(C_7H_8N_4)_6]$ $[BW_{12}O_{40}]{\bullet}1.5H_2O$	High purity CO_2 was the substrate. The CH_3CN was the solvent. TEOA was the sacrificial agent, and $[Ru(bpy)_3]Cl_2$ was the photosensitizer	Visible light	93.4%	[31]
g-C_3N_4 modified with POM	$Na_{10}Co_4(H_2O)_2(PW_9O_{34})_2$	The substrate was pure CO_2 purged in a mixture of acetonitrile, triethanolamine, $CoCl_2$, and bipyridine solution	Visible radiation with wavelength > 420 nm	94%	[32]

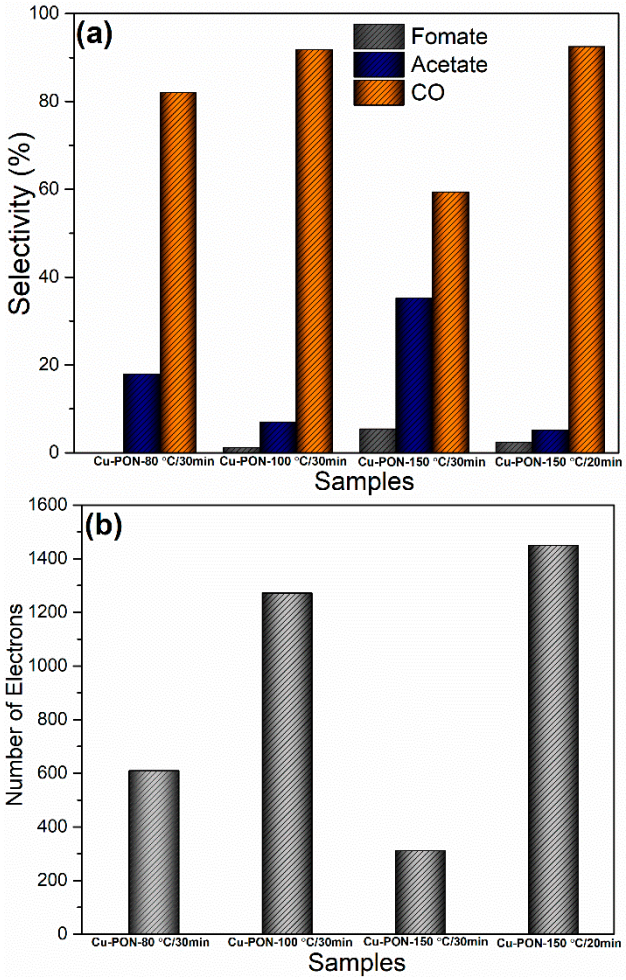

Figure 7. Selectivity of the copper-modified catalysts (**a**) and the number of electrons involved in the CO_2 photoreduction process (**b**).

Although some of the papers cited on Table 3 presented higher selectivity for CO than the present work, all of them use some photosensitizer, for instance, $[Ru(bpy)_3]Cl_2$ to enhance the photocatalyst activity. To be able to get a selectivity above 90% without using any photosensitizer or sacrificial agent is clearly an advantage of the $Na_7(H_3O)Nb_6O_{19}{\cdot}14H_2O$ prepared in this paper.

CO is a gas with a wide range of applications in the industrial sector, either in its pure form or as a synthesis gas. For example, the synthesis of formic acid by hydrolyzing methyl formate and the preparation of acetic acid by catalytic carbonylation of methanol are two of the main applications of CO, consuming more than 500,000 and 450,000 tons of pure CO annually, respectively [28]. Other applications are in the reaction of CO with chlorine to produce phosgene, which is a reagent used in the production of polyurethane and polycarbonate plastics and in the process of reducing oxides to metals in blast furnaces in steel mills [33].

The routes most used by the industrial sector for the production of CO on a large scale are coal gasification, the steam reforming process of natural gas or light hydrocarbons and partial oxidation of hydrocarbons [33]. However, these processes go against the trend of decarbonization of industrial processes. Thus, a low-carbon solution for carbon monoxide production is through the CO_2 photoreduction process, which has the potential to significantly change the structure of the carbon monoxide market by making CO production less centralized, in which small industrial plants can produce CO at the point of use, thus replacing the need for transport and large storage tanks, which are one of the major problems in the use of CO due to its toxicity and flammability.

The CO_2 photoreduction process occurs in different stages that involve adsorption, activation, and dissociation of the C-O bond, in which the activation of this molecule is one of the greatest challenges since CO_2 is highly stable and inert. Thus, one of the primary steps in the CO_2 reduction process is the adsorption of the CO_2 molecule on the surface of the material. The CO_2 molecule's interaction with the material's surface results in the production of the partly charged species $CO_2^{\delta-}$. Ref. [34] Each oxygen atom in the linearly arranged CO_2 molecule has a single pair of electrons available for donation to the Lewis acid sites on the surface of the catalysts. The carbon atom of the CO_2 molecule, on the other hand, can accept these electrons if the materials include Lewis base sites, generating carbonate-like species [35]. Additionally, if the semiconductor contains both basic and acid sites, it can work as both an electron donor and acceptor at the same time, creating mixed coordination with the CO_2 molecule.

In this way, based on the properties of polyoxoniobates together with the results of the photocatalysis, a mechanism for the catalytic photoreduction of CO_2 into CO, $HCOO^-$ and CH_3COO^-, through the interaction of the CO_2 with the surface of the material was proposed (Figure 8). Initially, we need to consider that polyoxoniobates predominantly have Lewis basic sites on their surfaces [36,37], which can donate a pair of electrons to the carbon atom of CO_2, which subsequently goes through two successive stages of protonation for the conversion of CO_2 to CO (Figure 8a) [38,39], with CO identified in many works as an intermediate of other products in the CO_2 photoreduction process, such as in the formation of CH_3COO^- (Figure 8c) [40,41]. On the other hand, the Lewis acid sites on the surface of polyoxoniobates can form a coordination with the oxygen of the CO_2 molecule upon receiving an electron pair, in which the coordination of oxygen favors the generation of the formate anion by favoring the bonding of H to the carbon of CO_2 (Figure 8b) [34,38].

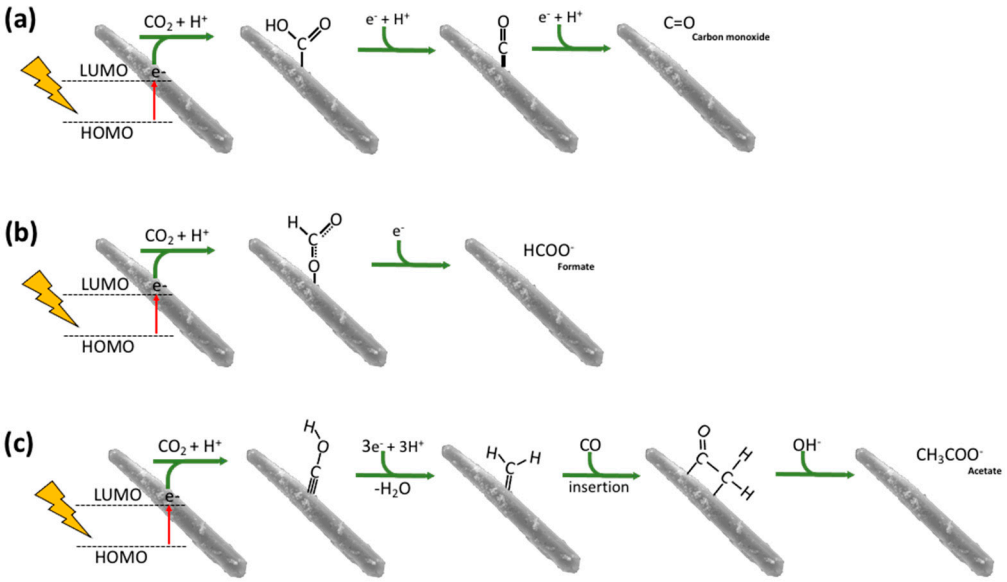

Figure 8. Schematic diagram for possible mechanisms for the reduction of CO_2 to CO (**a**), $HCOO^-$ (**b**), and CH_3COO^- (**c**).

In this way, the acid-base properties of the materials, which include type (Bronsted acid/base [proton donors/acceptors] vs. Lewis acid/base [electron donors/acceptors]), strength, concentration, and location, are characteristics that directly affect activity and selectivity during catalytic reactions [41–43].

4. Conclusions

Photocatalysts based on copper-modified polyoxoniobate were synthesized with low processing time and temperature through the coprecipitation method followed by microwave-assisted hydrothermal treatment. To determine conclusively whether Cu has

been incorporated into the polyoxoniobate structure as a doping ion or a counter-ion, techniques capable of probing the Cu coordination environment and oxidation state, such as X-ray absorption spectroscopy (XAS) and electron energy loss spectroscopy (EELS), would be required. However, we have enough evidence to suggest that Cu acts as a doping ion rather than a counter-ion. For instance, Figure 4's EDS mapping shows that Cu is homogeneously distributed in the polyoxoniobate structure, which is similar to Nb. Additionally, the presence of Cu in the material during elemental analysis suggests that it has been incorporated into the polyoxoniobate structure as a doping ion. Finally, the absence of CuO in the final material, as previously explained, indicates that Cu^{2+} is not a counter-ion, considering the highly alkaline synthesis conditions. To summarize, although we lack conclusive evidence of Cu^{2+} behavior as a doping ion, several experimental observations point to this conclusion.

In the CO_2 photoreduction process using these photocatalysts in a batch photoreactor, carbon monoxide, acetic acid, and formic acid were formed, while CO was the main product obtained by all photocatalysts. Changing the synthesis time altered the amount of copper present in the material, leading to greater activity and selectivity in the conversion of CO_2 to CO (92.5%). In addition, it is observed that the presence of a greater amount of copper in the structure of the material led to greater production of acetic acid. Thus, this work provides important information about the synthesis, activity, and selectivity of polyoxoniobate in the process of photocatalytic CO_2 reduction.

Supplementary Materials: The following supporting information can be downloaded at: https://www.mdpi.com/article/10.3390/appliedchem3020020/s1, Figure S1: Flowchart of the synthesis process to obtain the pristine polyoxoniobate modified with copper. Figure S2: Flowchart of the synthesis process to obtain the pristine polyoxoniobate. Figure S3: EDS spectra of the synthetized materials: (a) PON-150 °C/30 min, (b) Cu-PON-80 °C/30 min, (c) Cu-PON-100 °C/30 min, (d) Cu-PON-150 °C/30 min, and (e) Cu-PON-150 °C/20 min. Figure S4: NMR spectrum acetate obtained in the liquid phase after CO_2 photoreduction with Cu-PON-80 °C/30 min. Figure S5: NMR spectrum of the products obtained in the liquid phase after CO_2 photoreduction with Cu-PON-150 °C/30 min: (a) acetate and (b) formate, Figure S6: NMR spectrum of the products obtained in the liquid phase after CO_2 photoreduction with Cu-PON-150 °C/20 min: (a) acetate and (b) formate. Figures S7 to S12 SEM images and particle size distribution histograms for the Cu-PONs. Figure S13: XPS survey and Cu2p spectra of the Cu-PON-150 °C/30 min sample.

Author Contributions: Conceptualization, J.R.C.S. and A.E.N.; methodology, J.R.C.S., J.A.T., L.S.R., J.B.G.F. and F.L.S.; validation, J.R.C.S., J.A.T., L.S.R., J.B.G.F. and F.L.S.; formal analysis, J.R.C.S., J.A.T., L.S.R., J.B.G.F., F.L.S., N.M., L.F.G. and A.E.N.; resources, A.E.N.; writing—original draft preparation, A.E.N., L.F.G. and A.H.P.; writing—review and editing, A.E.N., L.F.G., N.M. and A.H.P.; supervision, A.E.N.; project administration, A.E.N.; funding acquisition, A.H.P. and A.E.N. All authors have read and agreed to the published version of the manuscript.

Funding: The authors are grateful to FAPEMIG (grants #APQ-02075-21), National Council for Scientific and Technological Development-CNPq, Ministry of Science, Technology and Innovation-MCTI (grants #406860/2022-0), and FAPESP (grants #2018/01258-5, #2018/12871-0) for financial support. The authors are also grateful to CAPES (Coordination for the Improvement of Higher Education Personnel—Finance Code 001).

Conflicts of Interest: The authors declare no conflict of interest.

References

1. Alsarhan, L.M.; Alayyar, A.S.; Alqahtani, N.B.; Khdary, N.H. Circular Carbon Economy (CCE): A Way to Invest CO_2 and Protect the Environment, a Review. *Sustainability* **2021**, *13*, 11625. [CrossRef]
2. Olah, G.A. Beyond Oil and Gas: The Methanol Economy. *Angew. Chem. Int. Ed. Engl.* **2005**, *44*, 2636–2639. [CrossRef] [PubMed]
3. Torres, J.A.; Cruz, J.C.; Nogueira, A.E.; Silva, G.T.S.T.; Oliveira, J.A.; Ribeiro, C. Role of Cu^0-TiO_2 interaction in catalyst stability in CO_2 photoreduction process. *J. Environ. Chem. Eng.* **2022**, *10*, 107291. [CrossRef]
4. Rawat, K.S.; Mahata, A.; Pathak, B. Thermochemical and electrochemical CO_2 reduction on octahedral Cu nanocluster: Role of solvent towards product selectivity. *J. Catal.* **2017**, *349*, 118–127. [CrossRef]

5. Silva, G.; Lopes, O.; Dias, E.; Torres, J.; Nogueira, A.; Faustino, L.; Prado, F.; Patrocínio, A.; Ribeiro, C. Redução de CO_2 em hidrocarbonetos e oxigenados: Fundamentos, estratégias e desafios. *Quím. Nova* **2021**, *44*, 963–981. [CrossRef]
6. Sharma, D.; Sharma, R.; Chand, D.; Chaudhary, A. Nanocatalysts as potential candidates in transforming CO_2 into valuable fuels and chemicals: A review. *Environ. Nanotechnol. Monit. Manag.* **2022**, *18*, 100671. [CrossRef]
7. Liu, Q.; Wang, X. Polyoxometalate Clusters: Sub-nanometer Building Blocks for Construction of Advanced Materials. *Matter* **2020**, *2*, 816–841. [CrossRef]
8. Zhang, M.; Li, H.; Zhang, J.; Lv, H.; Yang, G.Y. Research advances of light-driven hydrogen evolution using polyoxometalate-based catalysts. *Chin. J. Catal.* **2021**, *42*, 855–871. [CrossRef]
9. Gu, J.; Chen, W.; Shan, G.-G.; Li, G.; Sun, C.; Wang, X.-L.; Su, Z. The roles of polyoxometalates in photocatalyticarbontion of carbono dioxide. *Mater. Today Energy* **2021**, *21*, 100760. [CrossRef]
10. Aureliano, M.; Gumerova, N.I.; Sciortino, G.; Garribba, E.; Rompel, A.; Crans, D.C. Polyoxovanadates with emerging biomedical activities. *Coord. Chem. Rev.* **2021**, *447*, 214143. [CrossRef]
11. Ross, N.; Nqakala, N.; Willenberg, S.; Sifuba, S.; Iwuoha, E. Electrochemical Properties of Polyoxometalate (H3PMo12O40)-Functionalized Graphitic Carbon Nitride (g-C_3N_4). *Electrocatalysis* **2019**, *10*, 392–398. [CrossRef]
12. Hervé, G.; Tézé, A.; Contant, R. General Principles of The Synthesis of Polyoxometalates in Aqueous Solution. In *Polyoxometalate Molecular Science*; Borrás-Almenar, J.J., Coronado, E., Müller, A., Pope, M., Eds.; NATO Science Series; Springer: Dordrecht, The Netherlands, 2003; p. 98.
13. Nyman, M. Polyoxoniobate chemistry in the 21st century. *Dalton Trans.* **2011**, *40*, 8049. [CrossRef]
14. Niu, J.; Fu, X.; Zhao, J.; Li, S.; Ma, P.; Wang, J. Two-Dimensional Polyoxoniobates Constructed from Lindqvist-Type Hexaniobates Functionalized by Mixed Ligands. *Cryst. Growth Des.* **2010**, *10*, 3110–3119. [CrossRef]
15. Botar, B.; Ellern, A.; Hermann, R.; Kogerler, P. Electronic control of spin coupling in keplerate-type polyoxomolybdates. *Angew. Chem. Int. Ed.* **2009**, *48*, 9080–9083. [CrossRef]
16. Zhang, H.; Wang, T.; Chen, W. Polyoxometalate modified all-weather solar cells for energy harvesting. *Electrochim. Acta* **2020**, *330*, 135215. [CrossRef]
17. Liu, Z.Y.; Lin, Y.D.; Hao-Yu; Chen, H.N.; Guo, Z.W.; Li, X.X.; Zheng, S.T. Recent advances in polyoxoniobate-catalyzed reactions. *Tungsten* **2022**, *4*, 81–98. [CrossRef]
18. Shen, J.-Q.; Zhang, Y.; Zhang, Z.-M.; Li, Y.-G.; Gao, Y.-Q.; Wang, E.-B. Polyoxoniobate-based 3D framework materials with photocatalytic hydrogen evolution activity. *Chem. Commun.* **2014**, *50*, 6017–6019. [CrossRef]
19. Huang, P.; Qin, C.; Su, Z.-M.; Xing, Y.; Wang, X.-L.; Shao, K.-Z.; Lan, Y.-Q.; Wang, E.-B. Self-Assembly and Photocatalytic Properties of Polyoxoniobates: {$Nb_{24}O_{72}$}, {$Nb_{32}O_{96}$}, and {$K_{12}Nb_{96}O_{288}$} Clusters. *J. Am. Chem. Soc.* **2012**, *134*, 14004–14010. [CrossRef]
20. Makuła, P.; Pacia, M.; Macyk, W. How To Correctly Determine the Band GatoEnergy of Modified Semiconductor Photocatalysts Based on UV–Vis Spectra. *J. Phys. Chem. Lett.* **2018**, *9*, 6814–6817. [CrossRef]
21. Shen, L.; Xu, Y.Q.; Gao, Y.Z.; Cui, F.Y.; Hu, C.W. 3D extended polyoxoniobates/tantalates solid structure: Preparation, characterization and photocatalytic properties. *J. Mol. Struct.* **2009**, *934*, 37–43. [CrossRef]
22. Heng, S.; Song, Q.; Liu, S.; Guo, H.; Pang, J.; Qu, X.; Bai, Y.; Li, L.; Dang, D. Construction of 2D polyoxoniobate/RGO heterojunction photocatalysts for the enhanced photodegradation of tetracycline. *Appl. Surf. Sci.* **2021**, *553*, 149505. [CrossRef]
23. Nyman, M.; Alam, T.M.; Bonhomme, F.; Rodriguez, M.A.; Frazer, C.S.; Welk, M.E. Solid-state Structures and Solution Behavior of Alkali Salts of the $[Nb_6O_{19}]^{8-}$ Lindqvist Ion. *J. Clust. Sci.* **2006**, *17*, 197–219. [CrossRef]
24. Xu, H.; Nyman, M.; Nenoff, T.M.; Navrotsky, A. Prototype sandia octahedral molecular sieve (SOMS) $Na_2Nb_2O_6.H_2O$: Synthesis, structure and thermodynamic stability. *Chem. Mater.* **2004**, *16*, 2034–2040. [CrossRef]
25. Goiffon, A.; Philippot, E.; Maurin, M. Structure cristalline du niobate 7/6 de sodium $(Na_7)(H_3O)Nb_6O_{19}.14\ H_2O$. *Rev. Chim. Miner.* **1980**, *17*, 466–476.
26. Ma, P.; Wang, G.; Chen, G.; Wang, J.; Niu, J. A new two-dimensional polyoxoniobate built by Lindqvist-type polyoxoanion and copper coordinated cations $K_2[Cu(H_2O)_6]\{[Nb_6O_{19}][Cu(NH_3)]_2\}\cdot 8H_2O$. *J. Mol. Struct.* **2011**, *997*, 126–130. [CrossRef]
27. Quirino, M.R.; Lucena, G.R.; de Araújo, R.J.C.; da Silva, A.R.; de Melo, A.M.; dos Santos, I.M.G.; Gama, L. CuO and Ce-doped CuO Prepared by Microwave Hydrothermal Method in Photodegradation of Remazol Golden Yellow Dye. *Mat. Res.* **2023**, *26*, e20220300. [CrossRef]
28. Küngas, R. Review electrochemical CO_2 reduction for CO production: Comparison of low- and high-temperature electrolysis technologies. *J. Electrochem. Soc.* **2020**, *167*, 044508. [CrossRef]
29. Du, Z.-Y.; Yu, Y.-Z.; Li, N.-F.; Xue, Y.-S.; Xu, L.-X.; Mei, H.; Xu, Y. Polyoxomet-alate-Induced 'Cage-within-Cage' Metal–Organic Frameworks with High Efficiency towards CO_2 Photoreduction. *Sustain. Energy Fuels* **2021**, *5*, 3876. [CrossRef]
30. Qiao, L.; Song, M.; Geng, A.; Yao, S. Polyoxometalate-Based High-Nuclear Cobalt–Vanadium–Oxo Cluster as Efficient Catalyst for Visible Light-Driven CO_2 Reduction. *Chin. Chem. Lett.* **2019**, *30*, 1273–1276. [CrossRef]
31. Du, Z.-Y.; Xue, Y.-N.; Liu, X.-M.; Li, N.-F.; Wang, J.-L.; Mei, H.; Xu, Y. An Unprecedented Polyoxometalate-Encapsulated Organo–Metallophosphate Framework as a Highly Efficient Cocatalyst for CO_2 Photoreduction. *J. Mat. Chem. A* **2022**, *10*, 3469–3477. [CrossRef]
32. Zhou, J.; Chen, W.; Sun, C.; Han, L.; Qin, C.; Chen, M.; Wang, X.; Wang, E.; Su, Z. Oxidative Polyoxometalates Modified Gra-phitic Carbon Nitride for Visible-Light CO_2 Reduction. *ACS Appl. Mater. Interfaces* **2017**, *9*, 11689–11695. [CrossRef] [PubMed]

33. Kildahl, H.; Wang, L.; Tong, L.; Cao, H.; Ding, Y. Industrial carbon monoxide production by thermochemical CO_2 splitting—A techno-economic assessment. *J. CO_2 Util.* **2022**, *65*, 102181. [CrossRef]
34. Du, C.; Wang, X.; Chen, W.; Feng, S.; Wen, J.; Wu, Y.A. CO_2 transformation to multicarbon products by photocatalysis and electrocatalysis. *Mater. Today Adv.* **2020**, *6*, 100071. [CrossRef]
35. Dzade, N.Y. CO_2 and H_2O coadsorption and reaction on the low-index surfaces of tantalum nitride: A first-principles DFT-D3 investigation. *Catalysts* **2020**, *10*, 1217–1231. [CrossRef]
36. Cao, Y.; Chen, Q.; Shen, C.; He, L. Polyoxometalate-Based Catalysts for CO_2 Conversion. *Molecules* **2019**, *24*, 2069. [CrossRef] [PubMed]
37. Xu, Q.; Niu, Y.; Wang, G.; Li, Y.; Zhao, Y.; Singh, V.; Niu, J.; Wang, J. Polyoxoniobates as a superior Lewis base efficiently catalyzed Knoevenagel condensation. *Mol. Catal.* **2018**, *453*, 93–99. [CrossRef]
38. Ren, D.; Fong, J.; Yeo, B.S. The effects of currents and potentials on the selectivities of copper toward carbon dioxide electroreduction. *Nat. Commun.* **2018**, *9*, 925. [CrossRef]
39. Ci, C.; Carbó, J.J.; Neumann, R.; Graaf, C.; Poblet, J.M. Photoreduction Mechanism of CO_2 to CO Catalyzed by a Rhenium(I)−Polyoxometalate Hybrid Compound. *ACS Catal.* **2016**, *6*, 6422–6428. [CrossRef]
40. Nogueira, A.E.; Silva, G.T.S.T.; Oliveira, J.A.; Lopes, O.F.; Torres, J.A.; Carmo, M.; Ribeiro, C. CuO Decoration Controls Nb_2O_5 Photocatalyst Selectivity in CO_2 Reduction. *ACS Appl. Ener. Mater.* **2020**, *3*, 7629–7636. [CrossRef]
41. Sakhno, Y.; Bertinetti, L.; Iafisco, M.; Tampieri, A.; Roveri, N.; Martra, G. Surface hydration and cationic sites of nanohydroxyapatites with amorphous or crystalline surfaces: A comparative study. *J. Phys. Chem. C* **2010**, *114*, 16640–16648. [CrossRef]
42. Diallo-Garcia, S.; Osman, M.B.; Krafft, J.-M.; Casale, S.; Thomas, C.; Kubo, J.; Costentin, G. Identification of surface basic sites and acid–base pairs of hydroxyapatite. *J. Phys. Chem. C* **2014**, *118*, 12744–12757. [CrossRef]
43. Chong, R.; Fan, Y.; Du, Y.; Liu, L.; Chang, Z.; Li, D. Hydroxyapatite decorated TiO_2 as efficient photocatalyst for selective reduction of CO_2 with H_2O into CH_4. *Int. J. Hydrogen Energy* **2018**, *43*, 22329–22339. [CrossRef]